Digest Journal of Nanomaterials and Biostructures Vol. 19, No. 4, October-December 2024, p. 1665-1676

ZnO/CuO heterojunction prepared by sol-gel: characterization and photocatalytic evaluation

J. M. Rodríguez Valencia [a], E. Ramírez Morales [a], M. G. Hernandez Cruz [a], F. Servín de Dios [b], L. Rojas Blanco [a,*]

[a] *Autonomous Juarez University of Tabasco, University Avenue S/N, Magisterial Neighborhood, Villahermosa, Tabasco. ZC. 86040 Mexico.*

[b] *Academic Area of Earth Sciences and Materials, Institute of Basic Sciences and Engineering, Autonomous University of the State of Hidalgo, Pachuca-Tulancingo Highway km. 4.5, Mineral de la Reforma 42184, Hidalgo, Mexico*

ZnO, CuO and the ZnO/CuO heterojunction were prepared using zin acetate and copper acetate by sol-gel method. The materials were characterized by: TGA, XRD, XPS, SEM, TEM, EDS and UV-Vis. The heterostructure showed a synergistic effect compared to pure materials. The XPS results confirm the existence of a heterostructure. The morphology is a combination of characteristic morphologies of ZnO and CuO. The bandgap of ZnO decreases with the incorporation of CuO. The photocatalytic efficiency of the heterostructure increases; the degradation percentages were better for the heterostructures in both radiations: Ultraviolet and Visible.

(Received August 16, 2024; Accepted October 29, 2024)

Keywords: Zinc oxide, Copper oxide, Semiconductor, Photocatalysis, Organic dyes

1. Introduction

In recent years, water pollution has increased due to the large amount of toxic compounds discharged by industries such as the food, cosmetics, industrial, textile industry, etc [1]. Various methods have been established to reduce contamination, including: biological degradation [2], adsorption [3], solvent extraction and membrane separation [4]. However, these methods are inefficient because a second method is required to decontaminate. A promising alternative is Advanced Oxidation Processes (PAO), which are simple, stable and easy to implement. Heterogeneous Photocatalysis (HF) is part of the PAO, and is a technology based on illuminating a semiconductor material with a known amount of energy and generate hydroxyl radicals (•OH) and superoxides [3], which are highly reactive, non-selective and mineralize pollutants to CO_2, H_2O and other harmless compounds [5]–[7]. Various materials have been investigated for application as photocatalysts, however the zinc oxide (ZnO) is one of the most used due to its high photosensitivity in the range of 104-106 [8], low resistivity around 10-6 Ω [9], and high resistance to photocorrosion. The disadvantages of ZnO is a bandgap of 3.3 eV, photoactivity in the ultraviolet (UV) region and high electron recombination [10], [11]. [12].

To improve these limitations, ZnO is combined with metals such as Al and Ga [13] [14], and sensitized with other semiconductor oxides with a lower energy gap such as: SnO_2 [15], MgO [16], TiO_2 [17], Fe_2O_4[18] and CuO [19]. CuO is one of the most promising materials because is an economical, abundant and non-toxic material that is used to improve absorption in the visible region. CuO has shown to reduce the recombination time of the carriers and is effective in the degradation of organic contaminants.

In this work, the sol-gel synthesis of ZnO, CuO and ZnO/CuO powders and its characterization is reported. For the photocatalytic evaluation, methylene blue was used and two light sources were used: UV and Visible.

* Corresponding author: lizethrb@gmail.com
https://doi.org/10.15251/DJNB.2024.194.1665

2. Experimental

2.1. ZnO synthesis

The synthesis of ZnO was based on the methodology of Bharathi and collaborators [20]. Firstly, 50 ml of a 0.2 M solution of zinc acetate ($(CH_3COO)_2Zn \cdot 2H_2O$) was prepared, subsequently, a 0.2 M solution of sodium hydroxide (NaOH) with a molar concentration of 0.2 M was slowly added to a pH of 6 and then heated at 90 °C for 1 hour.

2.2. Synthesis of CuO

To synthesize CuO, 50 mL of copper acetate $Cu(CH_3COO)_2$ (0.2 M) was used and NaOH (0.2 M) was added and heated at 90 °C for one hour.

2.3. Synthesis of ZnO/CuO

To obtain the compound ZnO/CuO, $(CH_3COO)_2Zn \cdot 2H_2O$) 0.2 M (50 ml) were mixed and a solution of copper acetate ($Cu(CH_3COO)_2$) was slowly added to 0.2 M and was adjusted to a pH of 5.6 using a NaOH solution and then heated to 90° C for one hour.

2.4. Characterization

For TGA analysis, a TA Instruments Discover model is used from 30 to 600.00 °C with a ramp of 10.00 °C/min. For X Ray Diffraction, a Bruker diffractometer (D-8 Advance) was used at 40kV 30 mA with Cu Kalfa1 Tube and a step of 0.5 seconds. Thermo Fischer Scientific (K-alpha) device was used for the XPS analysis. A JEOL model JSM-7601F microscope is used for morphology analysis and a JEOL model JEM-2200FS microscope is used for TEM. The adsorption isotherms were obtained with a BEL JAPAN Brand equipment, model BELSORP-MAX-LP, degassed with nitrogen.

2.5. Photocatalytic tests

24 mg of photocatalyst in a methylene blue (MB) solution at 18 ppm were used. Two light sources were used for the photocatalytic evaluation: 20 W fluorescent lamp (Tecnolite) with $\lambda = 380$ nm and 14 W LED lamp with emission 400 nm to 750 nm and samples were taken every half hour for a total of 240 min.

3. Results and discussion

3.1. TGA analysis

Thermograms show a 15% weight loss before 90°C, which indicates the withdrawal of water (See Figure 1). The 67% of weight loss seen in the 145 - 340 °C range is attributed to the degradation of the precursor compounds that generate metal oxide; like that reported by Saravanan *et al.* [21] and by Munguti *et al.* [17]. No weight losses are observed after 340 °C, because the increase the annealing temperature improves the crystallinity of the material, and then the grains grow with less surface energy [14], [22]. These results allow us to elucidate the emergence of the compound(ZnO/CuO).

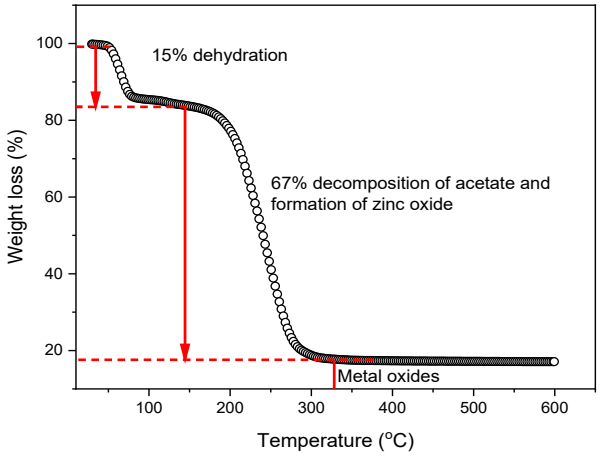

Fig. 1. Thermogram of the compound ZnO/CuO.

3.2. Structural analysis

In Fig. 2(a) the diffractogram of ZnO is observed with characteristic planes of the Hexagonal phase at 2θ = 31.77°, 34.37°, 36.22°, 47.53°, 56.59°, 62.85°, 66.45°, 67.99°, 69.03° , 72.55°, 76.99° of the diffracted planes: (100), (002), (101), (102), (110), (103), (200), (112), (201), (004) , (202) according to ICSD card No. 01-079-5604. The diffractogram of the CuO compound (Fig. 2(b)) shows peaks at 2θ = 35.51°, 38.64°, 48.76°, 53.43°, 58.36°, 61.25°, 66.18°, 72.27°, 74.88° corresponding to the planes diffracted from the monoclinic phase of CuO (ICSD No. 01-089-5896): (-111), (111), (-202), (020), (202), (-113), (-311), (311), (-222). Fig. 2(c) shows the diffractogram of the ZnO/CuO heterojunction where the hexagonal phase of ZnO and the monoclinic phase of CuO with the (-111) and (111) planes are observed. The inset in Fig. 2(c) shows the deconvolution of the (002) and (101) planes and where additional diffraction peaks are observed at 2θ = 35.55° and 38.82° associated with the monoclinic CuO phase.

The average crystal size was calculated using the Debye Scherrer (eq 1) where λ=1.5418 Å from CuKα, K(constant shape)=0.9 and β(mean maximum height)=FWHM.

$$D=\frac{k\lambda}{\beta\cos\theta} \tag{1}$$

The dislocation density (δ) [23] and the crystal lattice stress (ε) [24] of the (100), (002) and (101) planes of the phase ZnO hexagonal equations were calculated by equation 2 and 3:

$$\delta = \frac{1}{D^2} \tag{2}$$

$$\varepsilon = \frac{\beta}{4Tan\theta} \tag{3}$$

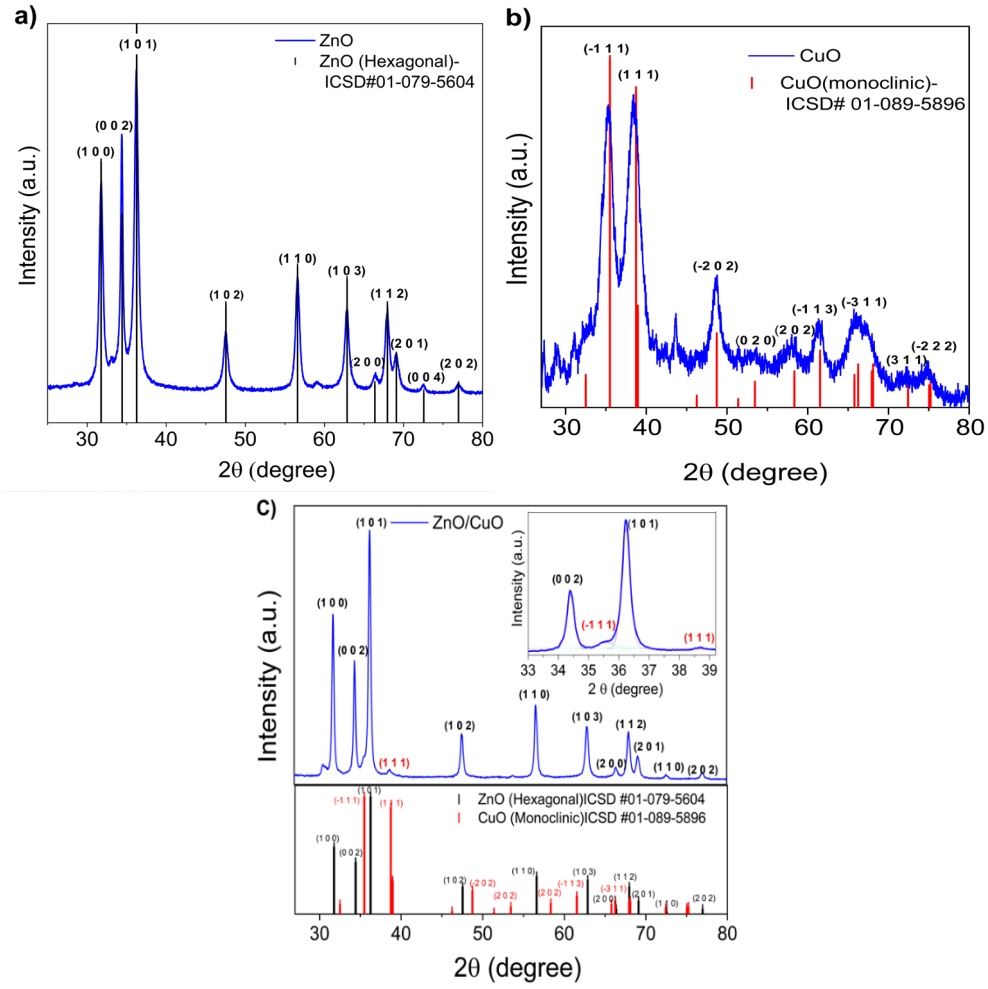

Fig. 2. Diffractograms of a) ZnO, b) CuO and c) ZnO/CuO.

Table 1 shows the calculated crystal sizes and stresses. For ZnO, values of 14.51 nm and 39.62 nm were obtained; for CuO of 10.18 nm and 5.19 nm of crystal size and stress respectively. The crystal size of the ZnO/CuO heterojunction was obtained as 25.21 nm. In the literature, crystal size values for ZnO/CuO are reported around 25 nm [23], [25]. The calculated values of **δ** and ε of the crystal lattice showed a decrease of 0.3 and 3.2 respectively. V. Kumari *et al.*, observed a decrease in ZnO with respect to the ZnO/CuO heterojunction of δ =0.5 and ε =1.2. This decrease suggests that the amount of defects, impurities, and vacancies located in the material and its grain boundaries also decreases [25].

The latticce parameters for ZnO were estimated: $a = \frac{\lambda}{\sqrt{3}Sin\theta}$; $c = \frac{\lambda}{Sin\theta}$ with a=b= 0.2861 Å and c=0.4956 Å. The ratio c/a=1.732, like what was reported for the hexagonal structure [23], [26]. The lattice parameters for CuO were calculated with: $\frac{1}{d^2} = \frac{1}{sin^2\beta}\left(\frac{h^2}{a^2} + \frac{k^2 sin^2\beta}{b^2} + \frac{l^2}{c^2} - \frac{2hl\ cos\beta}{ac}\right)$, where β=99.44° (ICSD No. 01-089-5896)(See table 1)

The Zn $2p_{3/4}$ and Zn $2p_{1/2}$ signals located around 1021 eV and 1044 eV respectively (figure 3b) confirm the presence of Zn^{+2}. The shift observed is attributed to a reaction in the heterostructure, in which the different electronegativities (Zn^{2+} =1.7 and Cu^{2+}=2.0) generate a heterojunction due to band doubling that balances with the Fermi level. [27], [28]. The deconvolution of the O 1s signal shows 2 peaks: the one at 530.16 eV is associated with Oxygen (O^{2-}) shared between the metal oxides of CuO and ZnO [27]. The peak at 531.72 eV is related to oxygen vacancies, which are electron donor states that allow increasing the lifetime of the carriers in oxidation and reduction reactions [29]. Figure 3d shows the Cu 2p signal with Cu $2p_{3/2}$ (932.27 eV) and Cu $2p_{1/2}$ (945.08 eV) signals of the Cu(II) oxidation state for CuO [27].

Table 1. Calculation of the crystallite size of the samples.

Samples	Lattice parameters (Å)			Miller plane	Crystal Size by Sherer	Crystal Corrected for strain	Lattice strain	Dislocation density
	a	b	c	(h k l)	(D) (nm)	(nm)	(x 10^{-3}) (ε)	(x 10^{-3}) (δ)
ZnO				1 0 0				
	0.2861	0.2861	0.4956	0 0 2	14.51	39.62	5.5	4.7
				1 0 1				
CuO				-1 1 1				
	0.4687	0.3459	0.5127	1 1 1	10.18	5.19	9.2	9.6
				-2 0 2				
ZnO/CuO				1 0 0				
	0.2859	0.2859	0.4953	0 0 2	25.21		5.2	1.5
				1 0 1				

3.3. XPS analysis

The binding energies of the Zn, O and Cu elements were confirmed in the samples (Figure 3). The signal of Cu $2p_{1/2}$ with low intensity due to the concentration used of Cu in the heterostructure [30].

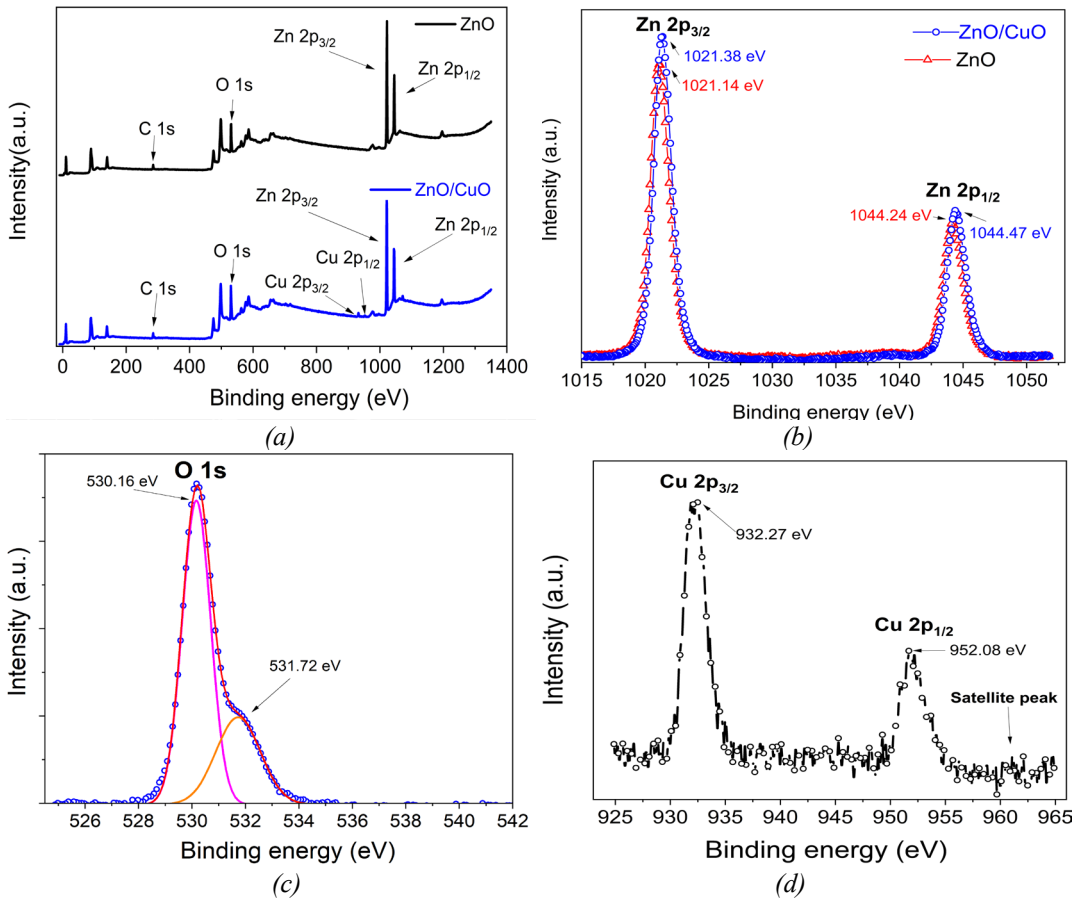

Fig. 3. XPS spectra of the a) Survey samples and signals of the elements b) Zn, c) O and d) Cu.

3.4. TEM analysis

The ZnO micrographs (Figure 4a) show rod-shaped grains with an average length of 146 ± 46 nm.

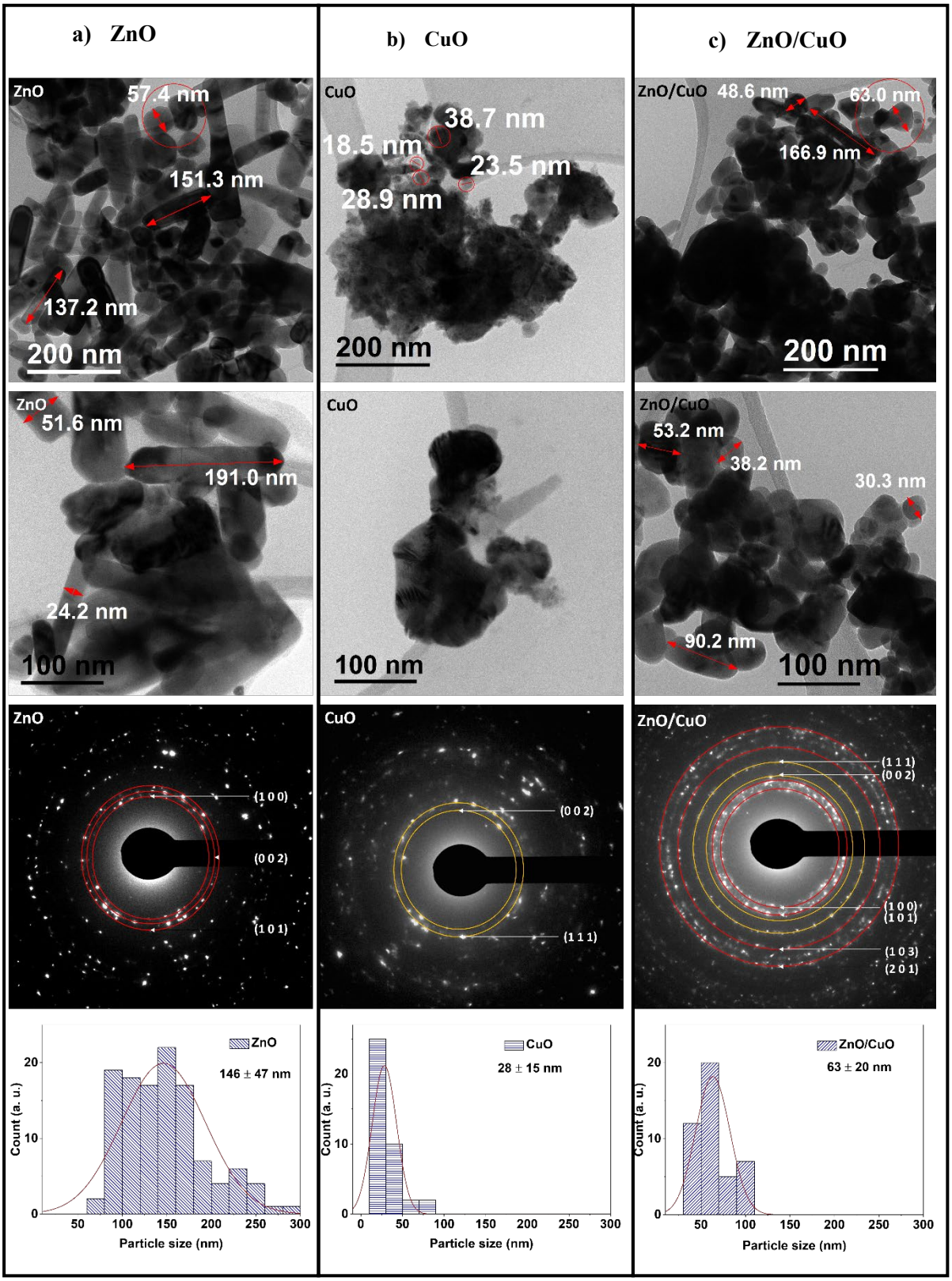

Fig. 4. TEM micrograph of a) ZnO, b) CuO and c) ZnO/CuO.

However, others are observed (marked with a red circle) with a diameter of 50 nm to 60 nm, indicating their incomplete nucleation. Fig. 4b of CuO shows clusters of agglomerated particles. According to E. Muchuweni et al., this particle agglomeration is attributed to surface roughness with disoriented active nucleation centers due to the high annealing temperature [31]. In the micrographs of the ZnO/CuO (Fig. 4c) a combination of rods and spheres with a particle size distribution of 63 ± 20 nm is observed. R. Saravanan et al. [21] and P. Bharathi, et al. [32] observed the same combination. The select area electron diffraction (SAED) patterns of ZnO were indexed to the principal intensities (1 0 0), (0 0 2) and (1 0 1) of ZnO (hexagonal) (ICCD No. 01-079 -5604) and monoclinic for CuO in planes (0 0 2) and (1 1 1) were identified (JPCDS No. 01-089-5896). In the ZnO/CuO diffraction pattern was indexed to the main planes of ZnO and CuO, finding the presence of particles of both phases that coexist in the analyzed sample.

3.5. Morphology analysis

A porous morphology is observed formed by the evaporation of organic precursors during thermal treatment [33]. The ZnO sample (see Figure 5a) presents grains with a length of 18±4 nm, while the ZnO/CuO sample presents a morphology of grains of 1.6 µm with others on the surface of 30±7 nm. EDS analysis confirms the presence of each of the elements of the synthesized compounds.

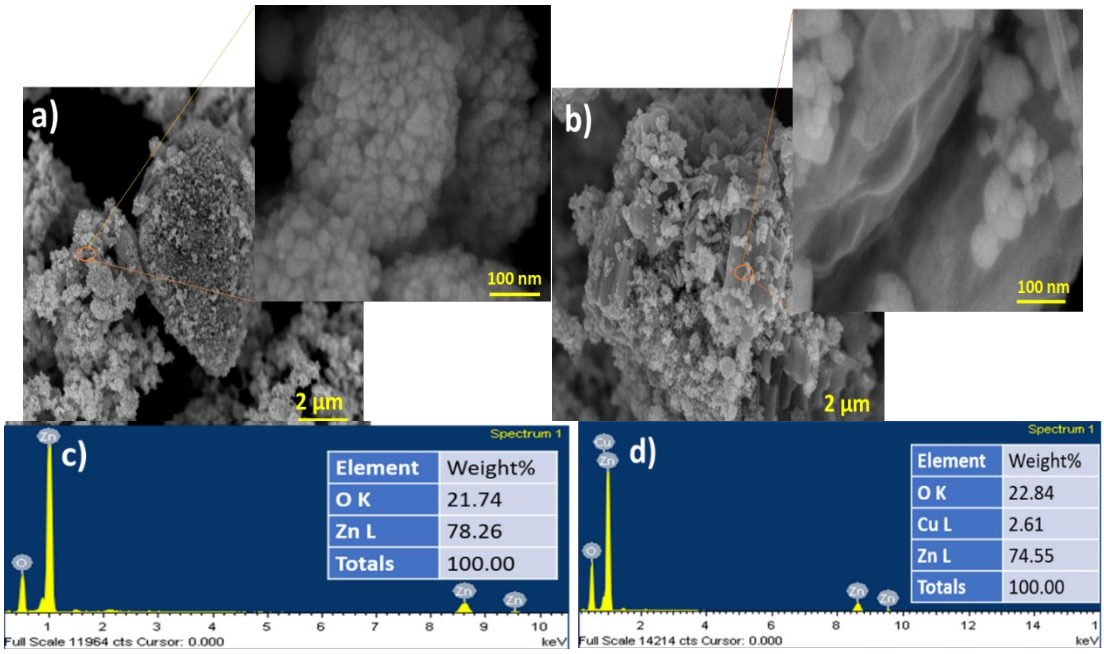

Fig. 5. a) SEM micrograph of ZnO and (b) ZnO/CuO. EDS analysis of c) ZnO and (d) ZnO/CuO.

3.6. Optical analysis

The absorption spectra of the samples are observed in Figure 6. To determine the band gap values of the samples, the Kubelka-munk F(R) function [35] was used (equation 4).

$$F(R) = \frac{\alpha}{S} = \frac{(1-R)^2}{2R} \tag{4}$$

where α=absorption coefficient, R=reflectance and S= dispersion factor (>5 µm) [36]. The α is related to the Photon´s energy(E), using the Tauc equation [37]:

$$\alpha = A(E - E_g)^n \tag{5}$$

where A= constant, Eg= band gap and n=direct or indirect electronic transition. The value of Eg was obtained by extrapolating the slope when α=0 from the graph $(F(R)h\nu)^2$ vs. hν. The estimated values

were 3.27 eV for ZnO, 2.2 eV for CuO and 3.25 eV for ZnO/CuO. In the literature, values of 3.37 eV and 3.12 eV are reported for ZnO [34], [38] and 2.4 eV and 2.1 for CuO [36], [39].

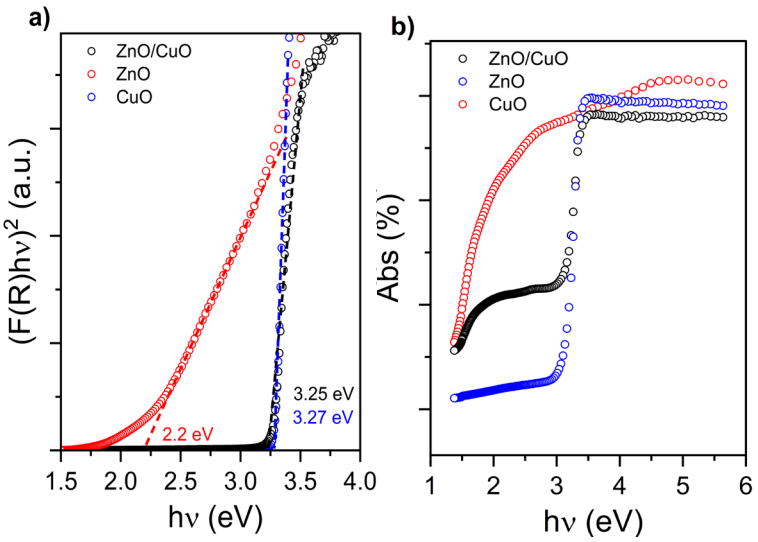

Fig. 6. a) Calculation of the bandgap of $(F(R)h\nu)^2$ vs hv and b) absorbance curves.

3.7. Photocatalytic activity

In the Figures 10a and 10b are observed absorption spectra under ultraviolet light and the Figures 10c and 10d are observed absorption spectra under visible light.

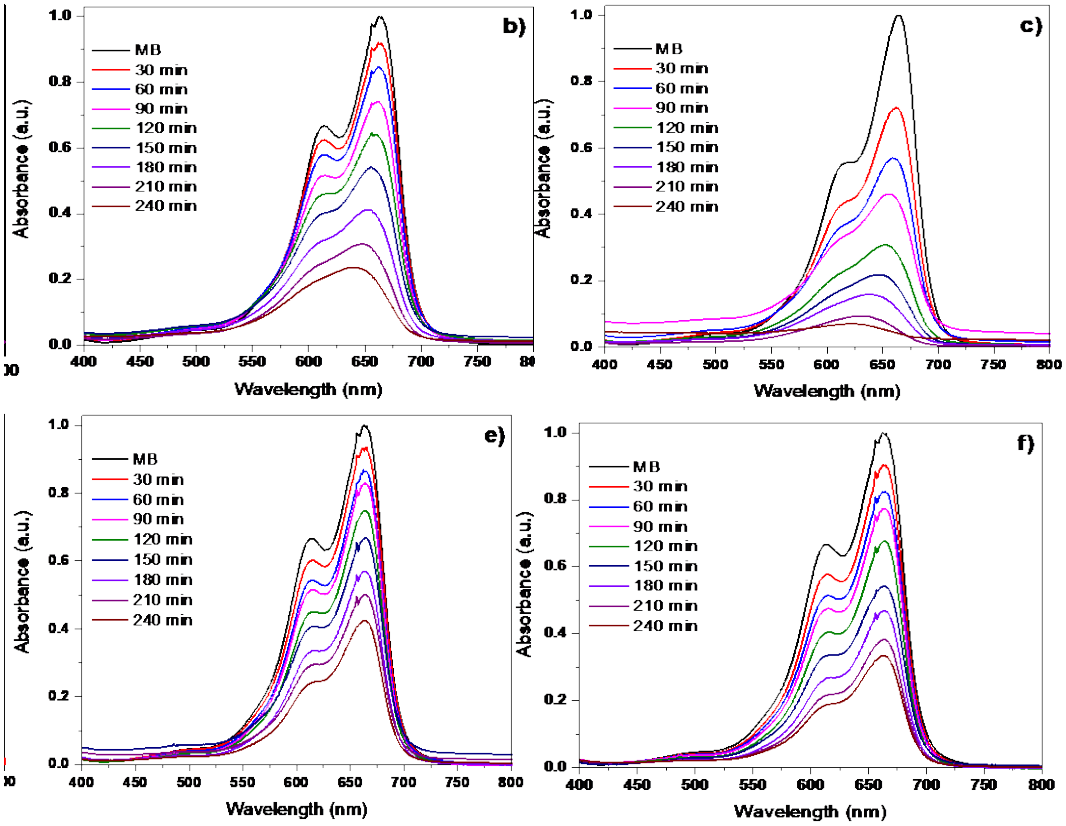

Fig. 10. Absorbance spectra using UV light of a) ZnO and b) ZnO/CuO and using visible light c) ZnO and d) ZnO/CuO.

The percentage of degradation or degradation efficiency is determined by the equation 6 [40].

$$\eta = \frac{C_0 - C}{C_o} * 100 \quad (6)$$

where C_0=is initial concentration and C= concentration at a given time.

The degradation efficiencies of the materials are shown in Figure 11. The comparison of ZnO and the heterojunction is observed using two radiation sources (UV and Visible) to achieve the photogeneration of its electrons. The degradation results for ZnO and ZnO/CuO irradiated with UV light were 81.87% and 95.94%, while for those irradiated with visible light they were 57.54% and 66.65%, respectively.

The results show that the heterojunction has better degradation efficiency with UV and Visible light, compared to ZnO. Which suggests that CuO improves the separation of carriers; and functions as a capture site for photoexcited electrons (trap) [41], [42]

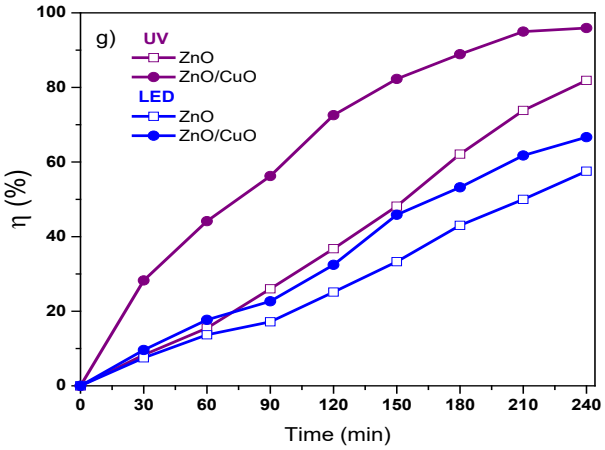

Fig. 11. Degradation efficiency using the two light sources.

To initiate the photocatalytic degradation process with the heterostructure, ZnO absorbs radiation to generate charge carriers (Equation 7), which follow different routes; the electrons that moved to the surface interact with oxygen and form superoxide radicals (Equation 8). On the other hand, the holes with water form hydroxyl radicals (Equation 9). All radicals in contact with the contaminating molecule cause mineralization (Eqs. 10 and 11) (see Figure 12a) [43].

Also, when carriers are generated in the heterostructure (Equation 12), the electron in the conduction band (CB) of ZnO following a Z scheme mechanism (Equation 13), this promotes separation of charges, achieving that the CuO electrons in the CB participate in the generation of $\bullet O_2^-$ (Equation 14) and the holes in the ZnO valence band (VB) generate $\bullet OH$ (Equation 15) (see Figure 12b) [44], [45], [46].

$$ZnO + hv \rightarrow ZnO\ (e_{CB}^- + h_{VB}^+) \quad (7)$$

$$e^- + O_2 \rightarrow \bullet O_2^- \quad (8)$$

$$h^+ + H_2O \rightarrow \bullet OH \quad (9)$$

$$\bullet O_2^- + MB \rightarrow H_2O + CO_2 \quad (10)$$

$$\bullet OH + MB \rightarrow H_2O + CO_2 \quad (11)$$

$$ZnO/CuO + hv \rightarrow ZnO(e_{CB}^- + h_{VB}^+) + CuO(e_{CB}^- + h_{VB}^+) \quad (12)$$

$$ZnO\ (e^-_{CB}) + CuO\ (h^+_{VB}) \rightarrow \text{recombination} \quad (13)$$

$$e^-_{CB\ (CuO)} + O_2 \rightarrow \bullet O_2^- \quad (14)$$

$$h^+_{VB\ (ZnO)} + H_2O \rightarrow \bullet OH \quad (15)$$

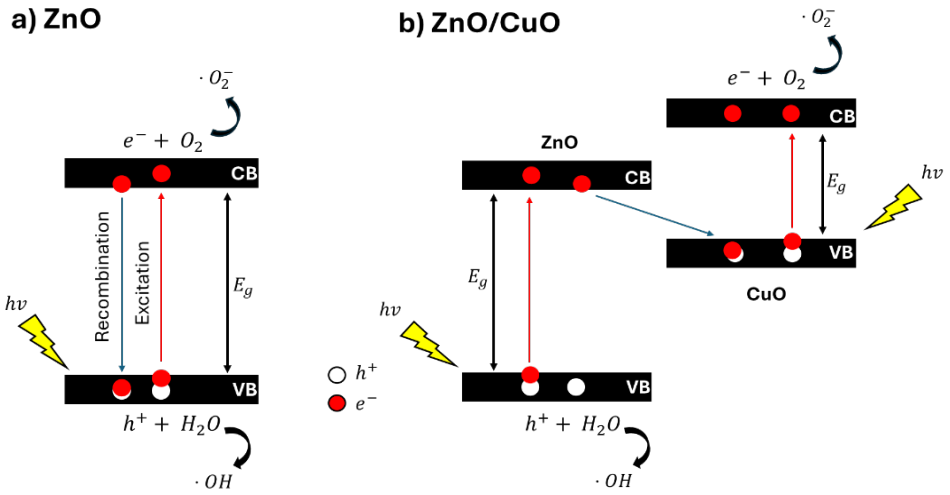

Fig. 12. Proposed charge transfer mechanism for a) pure ZnO and b) ZnO/CuO heterojunction [42], [45].

4. Conclusion

Complete removal of organic precursors by appropriate thermal treatments favoured the formation of ZnO, ZnO/CuO with a ladder-like interface between both metal oxides. The formation of a ZnO/CuO heterostructure with the appearance of the appropriate phases and morphologies allowed obtaining high photocatalytic efficiency using radiation sources in the visible and ultraviolet range.

Acknowledgements

J.M. Rodriguez Valencia acknowledges CONAHCyT, Mexico, for financial support through the fellowship.

Declaration of Competing interest

The authors of this paper declare no competing interest of personal, financial nor any kind that could influence this research.

References

[1] P. Bharathi et al., Appl Surf Sci, 484, 884 (2019); https://doi.org/10.1016/j.apsusc.2019.03.131

[2] D. Smazna, S. Shree, O. Polonskyi, S. Lamaka, M. Baum, J Environ Chem Eng, 7[2], 103016(2019); https://doi.org/10.1016/j.jece.2019.103016

[3] A. Fouda, S. S. Salem, A. R. Wassel, M. F. Hamza, T. I. Shaheen, Heliyon, 6[9], e04896 (2020); https://doi.org/10.1016/j.heliyon.2020.e04896

[4] L. Huang, F. Peng, F. S. Ohuchi, Surf Sci, 603[17], 2825(2009); https://doi.org/10.1016/j.susc.2009.07.030

[5] M. H. Ed et al., MBE Growth and Characterization of Long Wavelength Dilute Nitride III-V Alloys, 2005.

[6] X. Wang, S. Li, L. Xie, X. Li, D. Lin, Z. Zhu, Ceram Int, 46[10], 15858(2020); https://doi.org/10.1016/j.ceramint.2020.03.133

[7] L. Huang, F. Peng, F. S. Ohuchi, Surf Sci, 603[17], 2825(2009); https://doi.org/10.1016/j.susc.2009.07.030

[8] H. Kind, H. Yan, B. Messer, M. Law, P. Yang, Advanced materials, 14[2], 158(2002); https://doi.org/10.1002/1521-4095(20020116)14:2<158::AID-ADMA158>3.0.CO;2-W

[9] A. R. A. Rashid, H. K. Tazri, Nano Hybrids and Composites, Trans Tech Publ, 2021, pp. 25-33; https://doi.org/10.4028/www.scientific.net/NHC.31.25

[10] M. Weng et al., iScience, 24[8], 102884(2021); https://doi.org/10.1016/j.isci.2021.102884

[11] Y. Jiang et al., Cell Rep Phys Sci, 2[3], 100356(2021); https://doi.org/10.1016/j.xcrp.2021.100356

[12] A. Samad, M. Furukawa, H. Katsumata, T. Suzuki, S. Kaneco, J Photochem Photobiol A Chem, 325, 97(2016); https://doi.org/10.1016/j.jphotochem.2016.03.035

[13] L. Chabane, N. Zebbar, M. Kechouane, M. S. Aida, M. Trari, Thin Solid Films, 605, 57(2016); https://doi.org/10.1016/j.tsf.2015.10.063

[14] K. Ruangon, W. Khamon, W. Pecharapa, Mater Today Proc, 5[6] 14155(2018); https://doi.org/10.1016/j.matpr.2018.02.082

[15] S. Sudhaparimala, M. Vaishnavi, Mater Today Proc, 3[6] 2373(2016); https://doi.org/10.1016/j.matpr.2016.04.150

[16] M. Sangeeta et al., Mater Today Proc, 4[11], 11791(2017); https://doi.org/10.1016/j.matpr.2017.09.096

[17] L. Munguti, F. Dejene, Nano-Structures & Nano-Objects, 24, 100594(2020); https://doi.org/10.1016/j.nanoso.2020.100594

[18] A. Benaboud, M. Zaabat, M. S. Aida, B. Boudine, S. Benzitouni, T. Saidani, Optik (Stuttg), 144, 397(2017); https://doi.org/10.1016/j.ijleo.2017.06.108

[19] S. P. Mardikar, S. Kulkarni, P. V Adhyapak, J Environ Chem Eng, vol. 8, no. 2, p. 102788, 2020; https://doi.org/10.1016/j.jece.2018.11.033

[20] W. Lun, P. J. Mchugh, M. D. Symes, Chemical Engineering Journal, 444, 136573(2022); https://doi.org/10.1016/j.cej.2022.136573

[21] R. Saravanan, S. Karthikeyan, V. K. Gupta, G. Sekaran, V. Narayanan, A. Stephen, Materials Science and Engineering: C, 3[1], 91(2013); https://doi.org/10.1016/j.msec.2012.08.011

[22] T. P. Rao, M. C. S. Kumar, Journal of crystallization process and technology, vol. 2012, 2012.

[23] D. Saravanakkumar et al., OpenNano, vol. 4, 100025(2019); https://doi.org/10.1016/j.onano.2018.11.001

[24] V. Mote, Y. Purushotham, B. Dole, Journal of Theoretical and Applied Physics, 6[1], 6(202); https://doi.org/10.1186/2251-7235-6-6

[25] V. Kumari, S. Yadav, J. Jindal, S. Sharma, K. Kumari, N. Kumar, Advanced Powder Technology, 31[7], 2658(2020); https://doi.org/10.1016/j.apt.2020.04.033

[26] A. Samavati, A. F. Ismail, H. Nur, Z. Othaman, M. K. Mustafa, Chinese Physics B, 25[7], 77803(2016); https://doi.org/10.1088/1674-1056/25/7/077803

[27] X. Wang, S. Li, L. Xie, X. Li, D. Lin, Z. Zhu, Ceram Int, 46[10], 15858(2020); https://doi.org/10.1016/j.ceramint.2020.03.133

[28] L. Huang, F. Peng, F. S. Ohuchi, Surf Sci, 603[17], 2825(2009); https://doi.org/10.1016/j.susc.2009.07.030

[29] Y. Jiang et al., Cell Rep Phys Sci, 2[3], 100356(2021); https://doi.org/10.1016/j.xcrp.2021.100356

[30] M. Weng et al., iScience, 24[8], 102884(2021); https://doi.org/10.1016/j.isci.2021.102884

[31] E. Muchuweni, T. S. Sathiaraj, H. Nyakotyo, Mater Sci Semicond Process, 68, pp. 80(2017); https://doi.org/10.1016/j.mssp.2017.06.011

[32] P. Bharathi et al., Appl Surf Sci, 484, 884(2019); https://doi.org/10.1016/j.apsusc.2019.03.131

[33] L. Ma et al., Colloid Interface Sci Commun, 49, p. 100636(2022); https://doi.org/10.1016/j.colcom.2022.100636

[34] Y. Zhang, Y.-H. Wen, J.-C. Zheng, Z.-Z. Zhu, Appl Phys Lett, 94[11], 113114(2009); https://doi.org/10.1063/1.3104852

[35] I. Cherif, Y. O. Dkhil, S. Smaoui, K. Elhadef, M. Ferhi, S. Ammar, J Clust Sci, 34[1] 623(2023); https://doi.org/10.1007/s10876-022-02248-z

[36] A. A. Radhakrishnan, B. B. Beena, Indian J. Adv. Chem. Sci, 2[2], 158(2014).

[37] B. D. Viezbicke, S. Patel, B. E. Davis, D. P. Birnie III, Physica Status Solidi B, 252[8], 1700(2015); https://doi.org/10.1002/pssb.201552007

[38] B. Sotillo, M. E. Solana, P. Fernández, Materials Physics and Chemistry (TRANSFERRED), 1[1], (2018); https://doi.org/10.18282/mpc.v1i3.581

[39] H. Kidowaki, T. Oku, T. Akiyama, Journal of Physics: Conference Series, IOP Publishing, 2012, p. 12022; https://doi.org/10.1088/1742-6596/352/1/012022

[40] L. Xu, J. Su, G. Zheng, L. Zhang, Materials Science and Engineering: B, 248, p. 114405(2019); https://doi.org/10.1016/j.mseb.2019.114405

[41] F. A. Cataño, G. Cáceres, A. Burgos, R. S. Schrebler, Int J Electrochem Sci, 13[10], 9242(2018); https://doi.org/10.20964/2018.10.08

[42] S. Ruan, W. Huang, M. Zhao, H. Song, Z. Gao, Mater Sci Semicond Process, 107, p. 104835(2020); https://doi.org/10.1016/j.mssp.2019.104835

[43] J. P. Shubha et al., Arabian Journal of Chemistry, 16[3], 104547(2023); https://doi.org/10.1016/j.arabjc.2023.104547

[44] A. Zare, A. Saadati, S. Sheibani, Mater Res Bull, 158, p. 112048(2023); https://doi.org/10.1016/j.materresbull.2022.112048

[45] J. Trakulmututa, C. Chuaicham, S. Shenoy, A. Srikhaow, K. Sasaki, S. M. Smith, Opt Mater (Amst), 133, p. 112941(2022); https://doi.org/10.1016/j.optmat.2022.112941

[46] K. Mubeen et al., Journal of Saudi Chemical Society, 27[3], 101639(2023); https://doi.org/10.1016/j.jscs.2023.101639